# Empirically Derived Helicopter Response Model and Control System Requirements for Flight in Turbulence


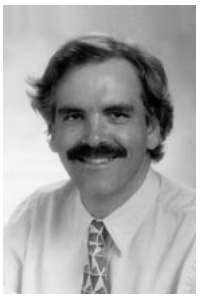


Jeff A. Lusardi  Mark B. Tischler  Chris L. Blanken  LCDR Steven J. Labows*

*Army/NASA Rotorcraft Division*
*Aeroflightdynamics Directorate (AMRDEC)*
*US Army Aviation and Missile Command, Moffett Field, CA*

*United States Navy*
*Naval Postgraduate School, Monterey, CA*



**Flight test data from a UH-60 Black Hawk helicopter in turbulent conditions were used to determine control system disturbance rejection criteria and to develop a low speed turbulence model for helicopter simulation. A system identification approach to modeling the aircraft response to turbulence was used to extract representative control inputs that accurately replicate the aircraft response to disturbances. Parametric turbulence models that have a Dryden-type form and are scalable for varying levels of turbulence were developed. Estimates of flight control bandwidth for precision hover in turbulence were determined to support disturbance rejection flight control design and handling qualities criteria.**


## Notation

| | |
|---|---|
| $C_{\mathrm{i}}$ | collective gust transfer function coefficient |
| $G_{\delta\delta}$ | autospectrum of controller input |
| $G_{\delta_g}$ | gust control transfer function |
| $G_f$ | inverse model stabilization filter |
| $G_{w_g}$ | gust transfer function (vertical) |
| $K_{\delta_g}$ | gust transfer function scale factor |
| $K$ | gust transfer function gain (in) |
| $L_{\mathrm{i}}$ | integral scale length (ft) |
| $\overline{L}$ | average integral scale length (ft) |
| $p_{\mathrm{AC}}$ | aircraft roll rate (deg/sec) |
| $q_{\mathrm{AC}}$ | aircraft pitch rate (deg/sec) |
| $r_{\mathrm{AC}}$ | aircraft yaw rate (deg/sec) |
| $S_{nn}$ | autospectrum of white noise source |
| $S_{w_g w_g}$ | autospectrum of vertical gust velocity |
| $U_o$ | longitudinal mean wind velocity (ft/sec) |
| $w$ | vertical turbulence velocity (ft/sec) |
| $w_{\mathrm{AC}}$ | aircraft vertical velocity (ft/sec) |
| $w_g$ | vertical gust velocity (ft/sec) |
| $\alpha_{\mathrm{i}}$ | temporal break frequency (rad/sec) |
| $\delta_{\mathrm{lat}}$ | pilot lateral cyclic deflection at aircraft mixer (in) |
| $\delta_{\mathrm{lon}}$ | pilot longitudinal cyclic deflection at aircraft mixer (in) |
| $\delta_{\mathrm{dir}}$ | pilot rudder deflection at aircraft mixer (in) |
| $\delta_{\mathrm{col}}$ | pilot collective deflection at aircraft mixer (in) |
| $\delta_{\mathrm{lat\text{-}G}}$ | equivalent gust lateral cyclic deflection at aircraft mixer (in) |
| $\delta_{\mathrm{lon\text{-}G}}$ | equivalent gust longitudinal cyclic deflection at aircraft mixer (in) |
| $\delta_{\mathrm{dir\text{-}G}}$ | equivalent gust rudder deflection at aircraft mixer (in) |
| $\delta_{\mathrm{col\text{-}G}}$ | equivalent gust collective deflection at aircraft mixer (in) |
| $\omega$ | observed angular frequency (rad/sec) |
| $\omega_{\mathrm{co}}$ | cut-off frequency (rad/sec) |
| $\sigma_{i_g}$ | RMS gust velocity (ft/sec) |
| $\Omega$ | spatial frequency (rad/ft) |
| $\tau_d$ | time delay (sec) |


Presented at the American Helicopter Society 56th Annual Forum, Virginia Beach, VA, May 2–4, 2000. Manuscript received May 2002; accepted June 2004.


*Currently with United States Navy, Commander, Naval Air Force, United States Atlantic Fleet, Norfolk, VA.

## Introduction

Helicopters operate in the lowest levels of the atmospheric boundary layer, often in turbulent conditions. As the level of wind and turbulence increases, task performance is compromised and pilot workload increases. The US Army handling qualities requirements for military rotorcraft, ADS-33E-PRF (Ref. 1), contains only a limited set of quantitative requirements that address response to turbulence. ADS-33 requires that pitch, roll, and yaw bandwidth for disturbance inputs meet the same specifications as the bandwidth for pilot control inputs (there are no disturbance rejection requirements for the heave axis). Flight test validation of these requirements was one of the key objectives of this study.

NRC Canada performed an initial disturbance-rejection handling qualities study (Ref. 2), but aside from their study, very few parametric wind/turbulence handling qualities studies exist. In fact, there are little or no supporting data for the disturbance rejection requirements in ADS-33. Reasons for the lack of data concerning wind and turbulence effects on rotorcraft have been that low speed, low altitude wind and turbulence models have been inadequate, not validated, or difficult to implement and use.

In the area of disturbance modeling, the traditional fixed-wing approach is to assume a spatially frozen gust pattern through which an aircraft flies, similar to a car driving down a bumpy road. The frequency content of the "frozen field" is often quoted in two forms, the von Karman and the more commonly used Dryden approximation (Ref. 3). The Dryden spectra are derived from observed exponential autocorrelations of turbulence measured in a wind tunnel. Extension to three dimensions has been carried out by applying the von Karman–Howarth relations for isotropic conditions (Ref. 4). The Dryden spectral models are a function of the aircraft velocity, which for fixed-wing aircraft is usually much greater than the mean wind speed. For rotorcraft hovering with respect

to the ground, the mean wind speed becomes the dominant velocity (Ref. 5).

Hess's analysis of rotorcraft handling qualities in turbulence utilizes a "frozen" turbulence field convecting at a given velocity toward the stationary vehicle (Ref. 6). He studied the effects of flight control characteristics on handling qualities in turbulence by including the effects of the turbulence gradients in an approximate fashion in the rotorcraft equations of motion. This approach served as a first-order correction to the approach typically used in the modeling of aerodynamic forces and moments due to turbulence for fixed-wing aircraft.

Another approach has been to model the turbulent flow field interaction with the helicopter using blade-centered and cyclo-stationary random processes (Ref. 7). This treatment of rotorcraft turbulence modeling, while valid, is complex in terms of modeling, tuning and implementation into ground or in-flight simulation.

To obtain an empirical rotorcraft turbulence model, NRC Canada used a variable stability Bell 205 helicopter to extract turbulence data directly from flight test (Ref. 2). To simulate a consistent level of disturbance, data from a flight in heavy turbulence (in the lee of a large building in strong winds) were used to determine the remnant aircraft response due to turbulence. These data were processed into a simple first-order inverse model of the aircraft to create equivalent actuator data traces. These could then be fed directly into the aircraft actuators to create a gust response. A technical approach similar to that used by NRC to extract equivalent gust data traces is employed in this study.

To achieve this, hover tasks were conducted on the leeward side of a cube-like aircraft hangar during moderate to strong wind conditions as shown in Fig. 1. The recorded flight data were analyzed to achieve two separate objectives. First, a cutoff frequency analysis of the measured pilot control inputs was conducted for comparison to the disturbance rejection requirements of ADS-33. Second, control positions that could be used to reproduce the portion of the aircraft rates due the gusts were extracted and used to develop gust models of a form similar to the Dryden spectral models.

This paper extends research conducted by Labows through the application of system identification techniques to the gust response modeling process and through the development of directional and collective gust models (Ref. 8). An overview of the method used to collect data from an instrumented UH-60 helicopter hovering in turbulence is described. An analysis of the flight data to determine control system bandwidths requirements to achieve a precision hover in turbulence is presented, and lastly, the paper develops scalable disturbance gust models for pitch, roll, yaw, and heave inputs.

**Fig. 1. UH-60 hovering on leeward side of Coast Guard Air Station hangar.**

**Table 1. Flight test condition**

| Flight number | OAT (°C) | Average wind velocity | | RMS gust velocity (ft/sec) |
|---|---|---|---|---|
| | | On roof (ft/sec) | At aircraft (ft/sec) | |
| 203 | 16 | 21.4 | 12.4 | 3.0 |
| 7-59 | 16 | 27.0 | 15.7 | 4.0 |
| 7-101 | 16 | 28.1 | 16.3 | 3.0 |
| 210 | 18 | 28.4 | 16.5 | 3.2 |
| 7-68 | 16 | 31.3 | 18.2 | 3.6 |
| 5 | 16 | 38.2 | 22.2 | 4.5 |
| 10 | 11 | 48.5 | 28.2 | 7.1 |

## Data Collection and Analysis

A UH-60A Black Hawk incorporating the External Stores Support System fixed provisions and fairings, reoriented production airspeed probes, and the modified production stabilator schedule was used (Ref. 9). The flight test site was the US Coast Guard Air Station at the San Francisco International Airport. The Air Station is at the north end of the airport, near the water's edge, and has a large ramp area surrounding the hangar on the leeward side. The hangar was approximately 40 feet high. Hover altitude was selected based on flow theory around blunt objects, and two hover tasks were conducted to different x–y position tolerance standards, tight ($\pm 5$ ft) and relaxed ($\pm 15$ ft), to capture varying levels of pilot control loop gain. Data were collected with the aircraft headed into the wind (On-axis) and perpendicular to the wind (Off-axis, Crosswind).

Wind speed and direction measurements were taken on the front edge of the hangar roof. The wind speeds were then corrected to the approximate hover location of the helicopter (Ref. 10). A summary of the flight test conditions is provided in Table 1. All frequency analyses were conducted using the Comprehensive Identification from FrEquency Responses (CIFER®) analysis tool, whose chirp-z transform and multi-window optimization provide improved spectral analysis when compared to fast Fourier transforms and single window spectral analysis (Ref. 11).

## Disturbance Rejection Analysis

In flight control modeling and design, a primary concern is the frequency range of controller input required to achieve a desired task performance. This is true for both piloted control and automatic control systems. Increasing the bandwidth of automatic control systems results in improved disturbance rejection. However, as bandwidth increases, so does sensor and actuator bandwidth requirements, the potential for undesirable interaction between the airframe structural modes and unmodeled dynamics, and susceptibility to interference from signal noise. Ultimately a trade-off is required in setting the crossover frequency to avoid the negative aspects of a high bandwidth control system while achieving satisfactory handling qualities.

### Cutoff frequency

A good estimate of the $-3$ dB control bandwidth (and crossover frequency) is the cut-off frequency, $\omega_{co}$, which is determined from a spectral analysis of the control deflection time history data $\delta(t)$ (Ref. 12). Cut-off frequency, or half-power frequency, is defined as the upper end of the frequency range that encompasses one-half of the total area under

**Table 2. Average cutoff frequencies (in rad/sec)**

| | | Flight 210 | | | | Flight 203 | | | |
|---|---|---|---|---|---|---|---|---|---|
| Position tolerance | | ±5 ft | | ±15 ft | | ±5 ft | | ±15 ft | |
| Input | Axis | Mean | | Mean | | Mean | | Mean | |
| | On | 2.75 | | 1.81 | | 1.87 | | 1.29 | |
| | On | 2.62 | | 1.72 | | | | 1.33 | |
| Longitudinal | On | 2.30 | 2.6 | 1.77 | 1.8 | | 1.9 | 1.38 | 1.3 |
| | Off | 2.51 | | 1.74 | | 1.87 | | 1.24 | |
| | Off | 2.58 | | 2.16 | | | | | |
| | On | 3.21 | | 1.96 | | 3.33 | | 1.93 | |
| | On | 3.73 | | 1.62 | | | | 0.95 | |
| Lateral | On | 3.91 | 3.7 | 2.42 | 2.0 | | 3.0 | 2.60 | 1.5 |
| | Off | 3.57 | | 1.92 | | 2.73 | | 0.65 | |
| | Off | 4.06 | | 2.30 | | | | | |
| | On | 1.57 | | 1.34 | | 1.04 | | 0.99 | |
| | On | 1.51 | | 1.11 | | | | 0.77 | |
| Directional | On | 1.75 | 1.6 | 1.19 | 1.2 | | 0.85 | 1.17 | 0.87 |
| | Off | 1.36 | | 1.26 | | 0.67 | | 0.55 | |
| | Off | 1.74 | | 1.31 | | | | | |

the measured autospectrum curve:

$$\frac{\int_0^{\omega_{co}} G_{\delta\delta}(\omega)\,\mathrm{d}\omega}{\int_0^{\infty} G_{\delta\delta}(\omega)\,\mathrm{d}\omega} = 0.5 \tag{1}$$

This is equivalent to the band limit that encompasses 70.7% (−3 dB) of the total control input Root Mean Squared (RMS), since the RMS ratio is the square root of the power ratio. The extracted pilot control input (at the mixer) cutoff frequencies ($\omega_{co}$) from two flights, 203 and 210, are summarized in Table 2. These results provide control system crossover frequency requirements as a function of turbulence level and accuracy (position tolerance).

The longitudinal mixer input cutoff frequencies are plotted against hover position tolerances for the stronger level of turbulence in Fig. 2, and the lighter level of turbulence in Fig. 3. Each bar in the plots represents approximately 90 sec of hover data taken at the indicated position tolerance. At the stronger level of turbulence (Fig. 2) the mean longitudinal cutoff frequency required to maintain a tight position tolerance (±5 ft) was 2.6 rad/sec, which decreased to 1.8 rad/sec for basic stabilization (±15 ft). At the lower level of turbulence (Fig. 3) the mean longitudinal cutoff frequency required to maintain a tight position tolerance (±5 ft)

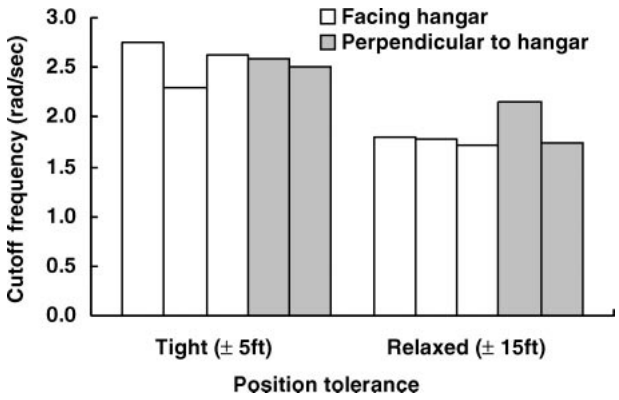


**Fig. 2. Longitudinal cutoff frequency differences for flight 210.**

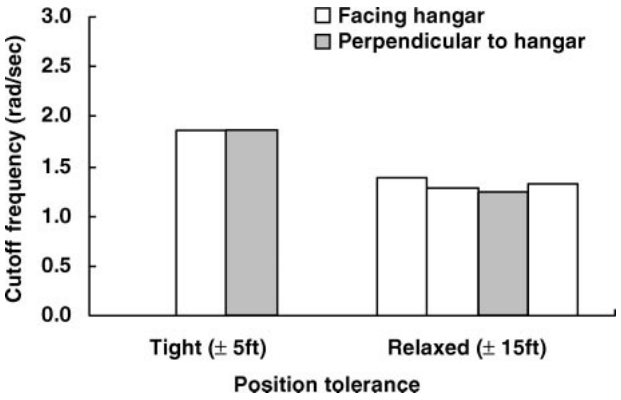


**Fig. 3. Longitudinal cutoff frequency differences for flight 203.**

was 1.9 rad/sec, which decreased to 1.3 rad/sec for basic stabilization (±15 ft). The figures show that the longitudinal cutoff frequency is independent of aircraft orientation. The figures also show that the longitudinal mixer input cutoff frequency increases with task demand and turbulence level. The same is true of the lateral and directional axes as indicated by the results tabulated in Table 2. These results confirm the assumption that with an increasing magnitude of disturbance response, an increasing pilot compensation level is required to achieve desired task performance (Ref. 2).

## Flight control requirements

Currently, ADS-33 disturbance rejection requirements state that pitch, roll, and yaw response bandwidths for inputs directly into the control surface actuators ($\theta/\delta_d$) shall meet the same bandwidth limits based on cockpit control inputs. These disturbance rejection bandwidth requirements are independent of turbulence level. The flight data from this study suggests otherwise. First, the previous results (Figs. 2 and 3) indicate that the pilot cockpit control cutoff frequency for a given tolerance is a function of the turbulence level. Secondly, disturbance rejection bandwidths are measured from inputs directly into the actuator, whereas the cockpit control input bandwidths ($\theta/\delta_s$) include delays and lags in the system between the pilot input and the aircraft response. Hence, disturbance rejection bandwidths ($\theta/\delta_d$) will generally have higher values than those from the cockpit controls ($\theta/\delta_s$), and simply applying the cockpit control bandwidth requirement may be too lenient.

An analysis was conducted to map the disturbance bandwidth as required in ADS-33, to the extracted control system cutoff frequencies ($\omega_{co}$) in Table 2. The mapping of bandwidth to cutoff frequency was obtained by tuning the flight control system crossover frequency of an Army/NASA variable stability UH-60 (Ref. 13) model to equivalent cutoff frequency values from the gust response flight test and then determining the resulting control system bandwidth. The variable stability control system is presented in Fig. 4, where M(s) contains stick filtering and desired

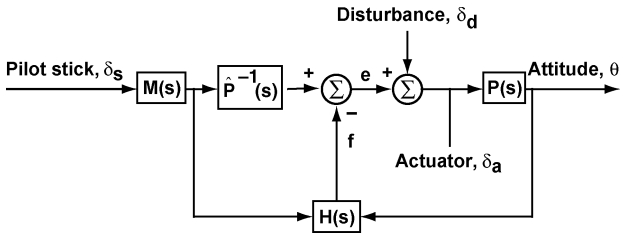


**Fig. 4. Variable stability model following control system.**

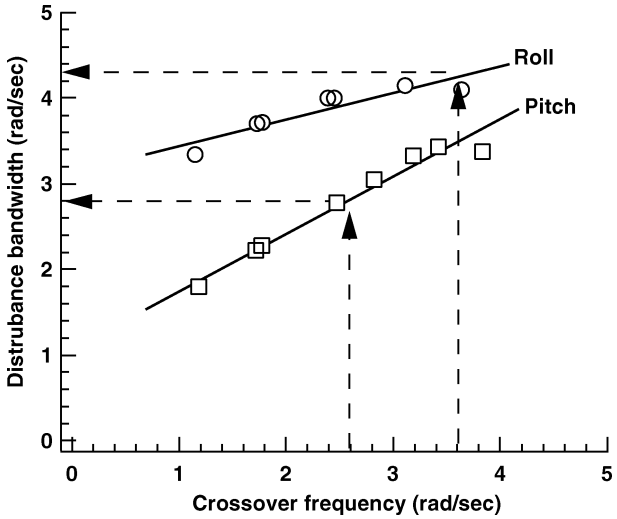


**Fig. 5. UH-60 disturbance bandwidth vs. control system crossover frequency.**

dynamics, P(s) is a model of aircraft dynamics, $\hat{P}^{-1}(s)$ is the approximate inverse of aircraft dynamics, and H(s) contains the feedback dynamics. From this control system schematic, bandwidth for handling-qualities response was obtained from $\theta(s)/\delta_s(s)$, bandwidth for disturbance response was obtained from $\theta(s)/\delta_d(s)$, and crossover frequency was obtained from f(s)/e(s). The pitch and roll results are shown in Fig. 5. The longitudinal cutoff frequency of 2.6 rad/sec and the lateral cutoff frequency of 3.7 rad/sec required to maintain a tight position tolerance in strong winds correspond to $(-135^\circ)$ disturbance bandwidth values of approximately 2.8 and 4.3 rad/sec, respectively. The bandwidth is defined as $(-135^\circ)$ phase point in the same closed-loop response, which will naturally occur at a higher frequency. The differences between the cutoff and bandwidth frequencies result from their definitions. For a typical feedback system equalized to a K/s broken-loop response, the cutoff frequency corresponds to the (−3dB) magnitude or the $(-45^\circ)$ phase point in the closed-loop response.

The pitch response disturbance bandwidth of 2.8 rad/sec and the roll disturbance bandwidth of 4.3 rad/sec are significantly higher than the current Level 1 boundaries of 1.0 and 2.0 rad/sec (Ref. 1). This indicates that the Level 1 gust response bandwidth requirements should be more stringent than the control response bandwidth requirements. Additional data will be needed to determine a generic boundary, but these results are useful for the Black Hawk class of utility vehicles.

## Gust Response Modeling

The process used to develop disturbance models started with the extraction of equivalent disturbance inputs from the flight data. This was accomplished by using the measured aircraft rates as inputs to the inverse of an identified model of the test aircraft. This produced a set of expected aircraft mixer inputs that if used as inputs to the identified model, would reproduce the same measured aircraft rates in the absence of turbulence. Subtracting the measured aircraft mixer inputs from the expected mixer inputs, resulted in remnant inputs that were essentially equivalent gust mixer inputs. A block diagram of the extraction process is shown in Fig. 6. The disturbance was then modeled using white-noise-driven shaping filters, of a form similar to the Dryden spectral models, designed to have power spectral densities equivalent to the power spectral densities of the extracted disturbance mixer inputs.

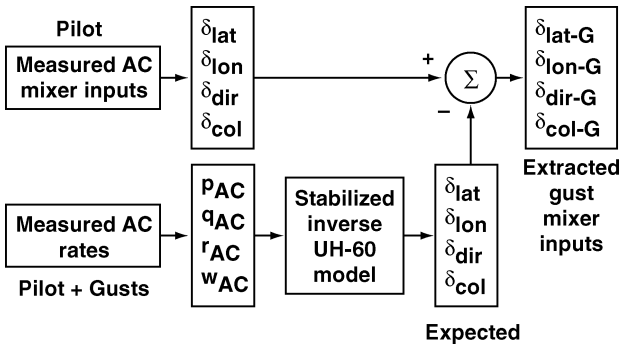


**Fig. 6. Extraction of gust mixer inputs.**

### Aircraft model

The aircraft model used in the gust extraction process was a fourteen-degree of freedom multiple-input–multiple-output (MIMO) model identified using CIFER® that is considered to be the most accurate model available (Ref. 14). This model characterizes the open loop UH-60 flight dynamics in hover over a frequency range of 0.5–40 rad/sec. The model includes fuselage dynamics, vertical inflow, rotor RPM, and engine/governor dynamics.

The aircraft model, which contains right half plane poles and transmission zeros, was inverted for use in the gust extraction process (Fig. 6). When the model was inverted, the model transmission zeros became the inverse model poles, and the model poles became the inverse model transmission zeros, which resulted in an improper, unstable inverse model. The inverse model was made proper by the addition of high frequency poles and stabilized by moving the right half plane poles to their mirror locations about the imaginary axis by applying the Padé type (all-pass) filter

$$G_f = \frac{(s^2 - 27.76s + 1077)(s^2 - 32.3s + 5035)}{(s^2 + 27.76s + 1077)(s^2 + 32.3s + 5035)} \tag{2}$$

to each of the 16 transfer functions of the inverse model. Addition of the high frequency poles and the filter did not affect the magnitude in the valid frequency range of the model (0.5–40 rad/sec), but did result in a phase shift introduced by the filter. The phase shift was approximated by an equivalent 65-msec time delay, $\tau_d = e^{-0.065s}$. To minimize the effects of the phase shift in the gust extraction process, the aircraft rate inputs to the inverse model were advanced by 65-msec (Ref. 15). A Bode plot analysis of the difference between the inverse model and the stabilized inverse model showed that the magnitude remained unchanged and the phase delay remained within acceptable limits up to a frequency of 40 rad/sec, which is the stated accuracy of the original UH-60 model.

### Gust remnant extraction and analysis

The next step in the modeling process was to extract the remnant aircraft control inputs as shown in Fig. 6. The extracted gust mixer input time histories were then bandpass filtered between 0.2 and 15 rad/sec to reduce the effects of low frequency drift in the open-loop time integration and the effects of high frequency measurement noise.

The autospectra of the extracted gust mixer inputs determined using CIFER® were examined for varying levels of pilot gain on flight events from the same flight (same level of turbulence) and are shown in Fig. 7. The coherence for each of the gust to pilot mixer input pairs is shown in Fig. 8. The generally higher coherence for the tight tolerance case indicates a higher correlation between the pilot inputs and the extracted gust remnants than for the relaxed tolerance case as expected. To minimize

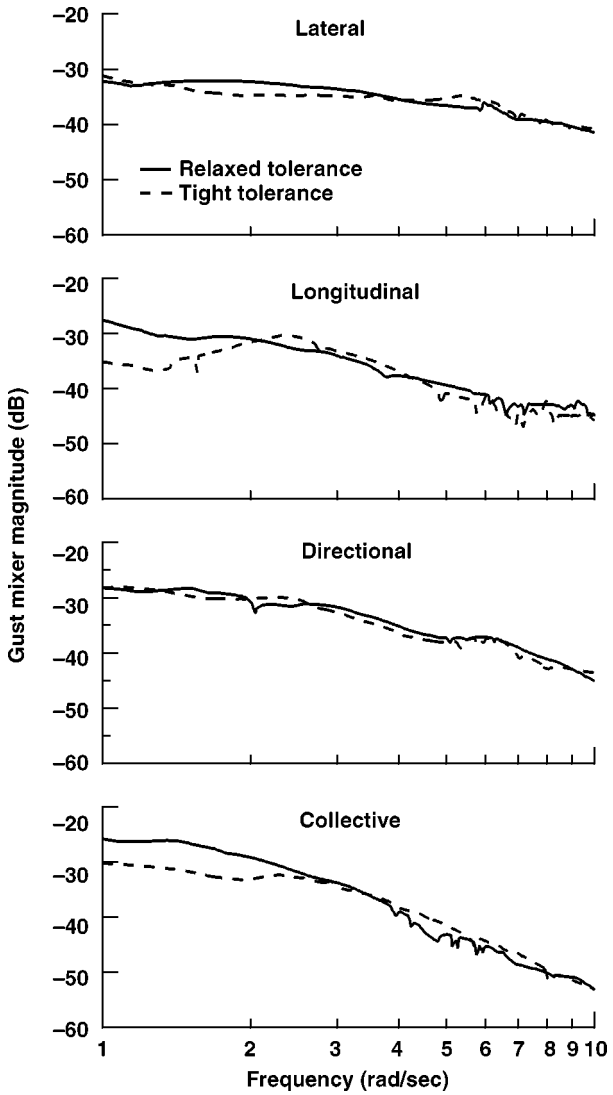


**Fig. 7. Gust mixer autospectra for varying pilot gain.**

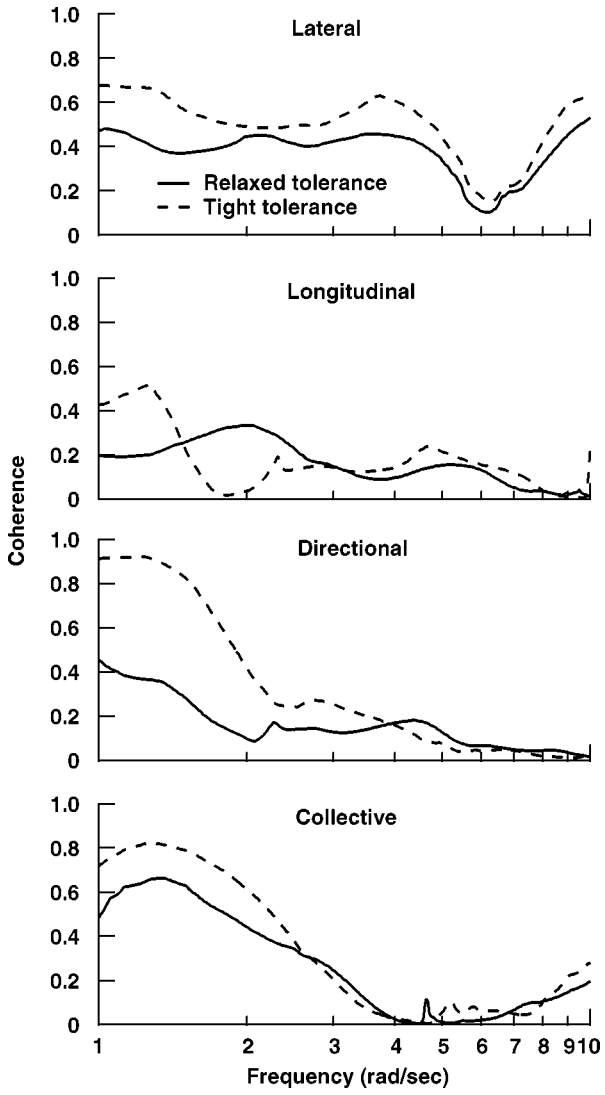


**Fig. 8. Coherence function for varying pilot gain.**

the correlation of the extracted gust remnants with pilot inputs, only the relaxed tolerance cases were used for the modeling process. This ensured that the remnants represented the true gust response and not modeling error or pilot remnants.

When examined for varying levels of turbulence, the autospectra of the gust mixer inputs followed the typical behavior of the autospectrum of atmospheric turbulence. A shift in the magnitude and break frequency for different turbulence levels is evident in the autospectrum plots of Fig. 9. Note that regardless of aircraft orientation, the autospectrum of the gust mixer input for each axis remained effectively the same as shown in Fig. 10. Independence of gust mixer input autospectra from aircraft orientation suggested turbulent mixing in all directions, which is consistent with the turbulent recirculating flows in bluff body wakes (Ref. 16). These results were also consistent with the cutoff frequency results (Figs. 2 and 3), which showed that the required pilot control cutoff frequencies were independent of aircraft orientation.

### Modeling gust mixer spectra

Rational transfer functions were developed to model the autospectra of the gust mixer inputs for use in simulation. These transfer functions produced autospectra equivalent to those of the extracted gust mixer inputs when driven by white noise inputs (e.g., Fig. 7). For modeling of atmospheric turbulence, classical methods utilize the von Karman power spectral density models (Ref. 7), which for the vertical gust velocity can be approximated by

$$S_{w_g w_g}(\Omega) = \left(\frac{4\sigma_{w_g}^2 L_u}{\pi}\right)\frac{1}{4+(L_u\Omega)^2} \tag{3}$$

where $\sigma_{w_g}^2 = \int_0^\infty S_{w_g w_g}(\Omega)\,\mathrm{d}\Omega$ as in Ref. 3, and $\Omega$ is the spatial frequency. The key model parameters are the vertical gust velocity RMS turbulence intensity ($\sigma_{w_g}$, ft/sec) and the scale length of the longitudinal turbulence ($L_u$, ft). Equation (3) can be re-written as

$$S_{w_g w_g}(\omega) = \left(\frac{L_u\sigma_{w_g}^2}{U_o\pi}\right)\left[\frac{1}{1+\left(\frac{\omega}{\alpha_u}\right)^2}\right] \tag{4}$$

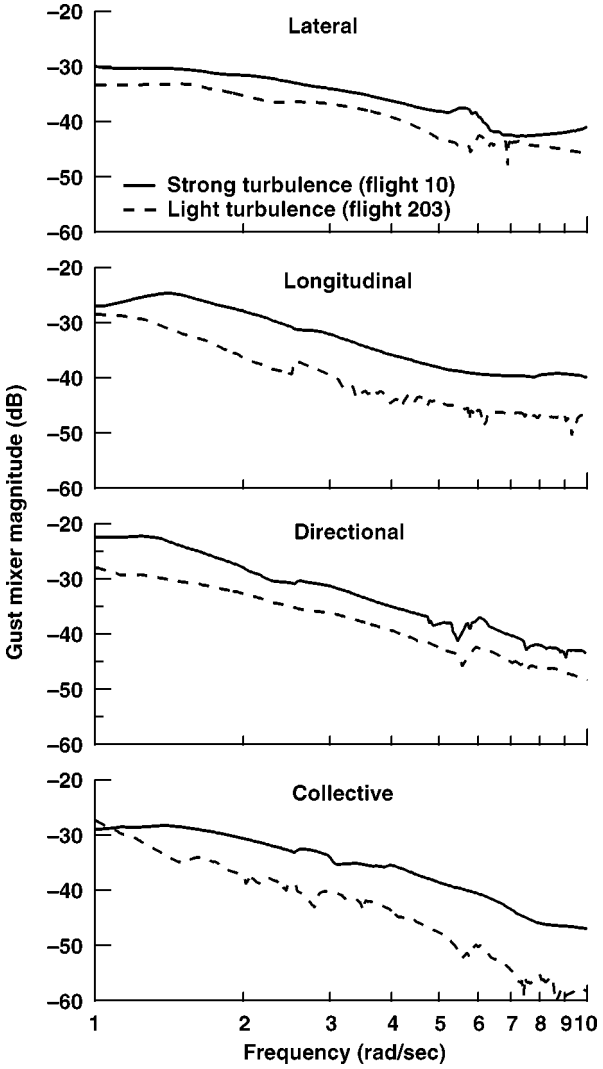


**Fig. 9. Gust mixer autospectra for varying turbulence levels.**

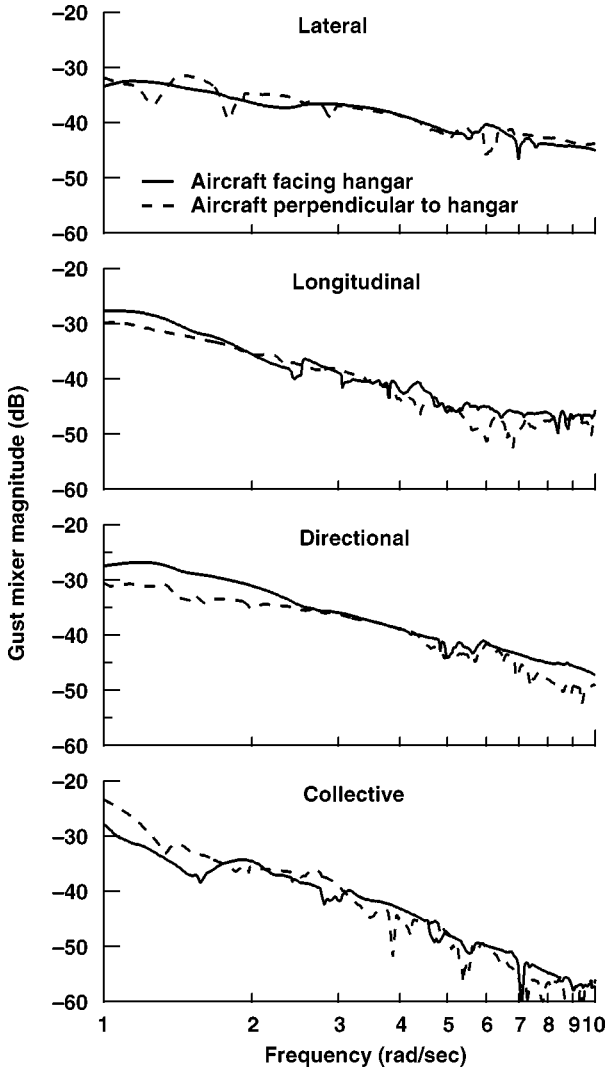


**Fig. 10. Gust mixer autospectra for varying aircraft heading orientation.**

where $\omega$ is the observed angular frequency given by

$$\omega = \Omega U_o \tag{5}$$

and $\alpha_u$ is the longitudinal power spectral density or autospectrum temporal break frequency given by

$$\alpha_u = \frac{2U_o}{L_u} \tag{6}$$

with turbulent mixing in all directions ($\sigma_u \approx \sigma_v \approx \sigma_w$) and the scale length relations $L_u = 2L_v = 2L_w$.

This approximation has the same form as the Dryden spectral model for longitudinal turbulence, but with one-half the scale length, as noted in Ref. 7. This spectral density function characterizes the mean squared value of the turbulence distribution with frequency. This specific form is presented in terms of the spatial frequency, $\Omega$, which is the observed angular frequency normalized by a reference airspeed. Whereas the Dryden form normalizes by the equilibrium speed of the aircraft, this research effort utilized a form similar to Hess (Ref. 6), were $U_o$ is the speed of the frozen field convecting past the stationary aircraft.

The gust transfer-function model, $G_{w_g}(\omega)$ consistent with Eq. (4) that produces the gust velocity ($w_g$) when driven by a random noise signal is given by

$$S_{w_g w_g}(\omega) = |G_{w_g}(\omega)|^2 S_{nn}(\omega) \tag{7}$$

where $S_{nn}(\omega) = 1$ for a white noise input. The required lateral and longitudinal transfer function determined from Eqs. (4) and (7) is then

$$G_{w_g}(s) = 2\sigma_u \left( \frac{\sqrt{\dfrac{U_o}{\pi L_u}}}{s + \alpha_u} \right) \tag{8}$$

This is a first-order transfer function model of the form

$$G_{w_g}(s) = \left( \frac{K}{s + \alpha} \right) \tag{9}$$

A plot of the autospectra of the extracted lateral, longitudinal and directional gust *mixer* inputs is shown in Fig. 11. The autospectra all exhibited essentially first-order characteristics. This indicated that these three gust mixer autospectra could be reproduced using white noise driven gust models of the same form as Eq. (9).

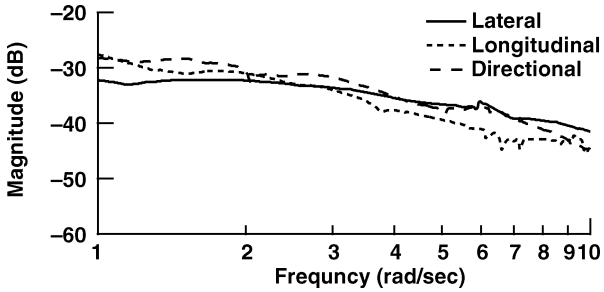


**Fig. 11. Lateral, longitudinal and directional gust mixer autospectra.**

To obtain a gust-control transfer function, $G_{\delta_g}$ that produced a gust-control autospectrum from a white noise input that matched the extracted gust mixer input autospectrum, Eq. (8) was matched with each autospectrum (e.g., Fig. 9) to determine the required scale factor $K_{\delta_g}$:

$$G_{\delta_g}(s) = K_{\delta_g}(2\sigma_u)\left(\frac{\sqrt{\dfrac{U_o}{\pi L_u}}}{s+\alpha_u}\right) \tag{10}$$

This provided the models for the lateral/longitudinal gust transfer functions. For the directional gust transfer function, $2L_v$ was substituted for $L_u$ in Eqs. (6) and (10).

Examination of the collective gust mixer autospectra indicated that a different form of the model should be used for the heave axis. Figure 12 shows a comparison of the collective and directional gust mixer autospectra. The form of the collective gust autospectrum is more consistent with a second order model then the first order model of Eq. (9). The form of the model selected for the collective gust input is based on the reduced order model of Ref. 17, and is given as

$$G_{\delta_g}(s) = K_{\delta_g}\frac{\sigma_{w_g}\sqrt{\dfrac{3U_o}{\pi L_w}}\left(s + C_1\dfrac{U_o}{L_w}\right)}{\left(s + C_2\dfrac{U_o}{L_w}\right)\left(s + C_3\dfrac{U_o}{L_w}\right)} \tag{11}$$

The modeling parameters $K$, and $\alpha$ were obtained using CIFER® by fitting Eq. (9) to the longitudinal, lateral and directional gust mixer autospectrum data (e.g., Fig. 9) using an optimization cost function. A cost of less than 100 is considered to be an acceptable fit and a cost of less then 50 an excellent fit (Ref. 11). The coefficient values and their respective costs are shown in Table 3. The lateral, longitudinal and directional turbulence scale lengths, $L_i$, were calculated based on the gust mixer autospectra break frequency results and Eq. (6) (with $2L_v = L_u$ for the directional fit).

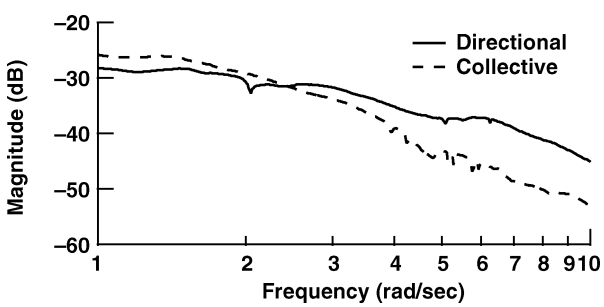


**Fig. 12. Directional collective and gust mixer autospectra.**

**Table 3. Spectral filter fit coefficients for gust mixer model**

| Flight | | $U_o$ (ft/sec) | $\sigma_{wg}$ (ft/sec) | $K$ (in) | $\alpha$ (rad/sec) | $L_i$ (ft) | Cost |
|---|---|---|---|---|---|---|---|
| 203 | (lat) | | | 0.43 | 1.32 | 18.9 | 33.9 |
| 203 | (lon) | 12.4 | 3.0 | 0.34 | 0.56 | 44.8 | 50.2 |
| 203 | (dir) | | | 0.43 | 0.51 | 24.6 | 9.2 |
| 7-59 | (lat) | | | 0.75 | 2.06 | 15.3 | 7.2 |
| 7-59 | (lon) | 15.7 | 4.0 | 0.83 | 1.35 | 23.3 | 40.0 |
| 7-59 | (dir) | | | 0.71 | 0.93 | 17.0 | 36.7 |
| 7-101 | (lat) | | | 0.76 | 2.22 | 14.7 | 6.6 |
| 7-101 | (lon) | 16.3 | 3.0 | 0.86 | 2.28 | 14.3 | 35.7 |
| 7-101 | (dir) | | | 0.75 | 0.75 | 21.8 | 38.9 |
| 210 | (lat) | | | 0.64 | 1.48 | 22.3 | 4.8 |
| 210 | (lon) | 16.5 | 3.2 | 0.57 | 1.27 | 26.0 | 5.3 |
| 210 | (dir) | | | 0.64 | 0.87 | 19.0 | 11.9 |
| 7-68 | (lat) | | | 0.85 | 2.22 | 16.4 | 7.8 |
| 7-68 | (lon) | 18.2 | 3.6 | 0.94 | 2.43 | 15.0 | 43.1 |
| 7-68 | (dir) | | | 0.72 | 1.03 | 17.7 | 15.3 |
| 5 | (lat) | | | 0.76 | 1.54 | 28.8 | 19.0 |
| 5 | (lon) | 22.2 | 4.5 | 0.74 | 1.97 | 22.6 | 40.3 |
| 5 | (dir) | | | 0.78 | 0.82 | 27.1 | 12.4 |
| 10 | (lat) | | | 0.68 | 1.66 | 34.0 | 8.8 |
| 10 | (lon) | 28.2 | 7.1 | 0.83 | 1.24 | 45.6 | 55.3 |
| 10 | (dir) | | | 0.78 | 0.69 | 40.7 | 41.8 |

The average value of $\bar{L} = 24.3$ feet is approximately equal to the rotor radius of the UH-60 helicopter (26.9 ft). This result is consistent with the modeling results of Costello et al. (Ref. 18). When fitting the gust transfer functions of Eq. (9) to the extracted gust autospectra, it was noted that the cost is least sensitive to the location of the break frequency coefficient $\alpha$, and most sensitive to the gain $K$, as would be expected given the first-order form of the extracted gust autospectrum plots (e.g., Fig. 11). For this modeling process, the variables that determine the break frequency $\alpha$ are the mean wind speed, $U_o$ and the scale length $L_i$. To achieve consistency in the gust models, the scale length for all of the models was set to $L_i = L = 26.9$ ft, which is the main rotor radius of the UH-60 helicopter.

The recalculated lateral, longitudinal and directional gust model transfer function coefficients based on a common scale length of 26.9 ft are tabulated in Table 4. The fit costs for all the fits in Table 4 remained within the acceptable range of less than 100. For the collective gust model, the mean wind speed $U_o$ and common scale length $L$ were used to obtain the constant coefficients $C_i$ of Eq. (11).

By specifying the value of the scale lengths, the transfer-function gains $K$ of the derived gust mixer transfer functions for the longitudinal and lateral data become nearly the same (Table 4). This led to the conclusion that the lateral and longitudinal models could be reduced to a single model that is dependant on the mean wind speed, gust turbulence intensity, and a common scale length. Since the longitudinal crossover frequency was approximately the same for headwind and crosswind conditions, it was surmised that the character of the aerodynamic moments due to turbulence is uniform for pitch, independent of aircraft orientation. This same logic applies to the lateral axis.

To a first approximation, the applied gust aerodynamic moments are the same for pitch and roll and are independent of aircraft orientation. Since the extracted pitch and roll gust mixer inputs are essentially simulated gust aerodynamic moments as produced from a circular rotor disc, they should be the same. The resulting aircraft response is the applied aerodynamic moment normalized by the associated inertia, so the effects

**Table 4. Spectral filter fit coefficients for gust mixer model with fixed $L_i$ = 26.9 ft**

| Flight | | $U_o$ (ft/sec) | $\sigma_{wg}$ (ft/sec) | $K$ (in) | $\alpha$ (rad/sec) | $L_i$ (ft) | Cost |
|---|---|---|---|---|---|---|---|
| 203 | (lat) | | | 0.39 | 0.93 | 26.9 | 45.7 |
| 203 | (lon) | 12.4 | 3.0 | 0.37 | 0.93 | 26.9 | 69.4 |
| 203 | (dir) | | | 0.43 | 0.46 | 26.9 | 9.5 |
| 7-59 | (lat) | | | 0.59 | 1.17 | 26.9 | 41.6 |
| 7-59 | (lon) | 15.7 | 4.0 | 0.79 | 1.17 | 26.9 | 42.3 |
| 7-59 | (dir) | | | 0.65 | 0.58 | 26.9 | 52.8 |
| 7-101 | (lat) | | | 0.58 | 1.22 | 26.9 | 48.0 |
| 7-101 | (lon) | 16.3 | 3.0 | 0.66 | 1.22 | 26.9 | 90.6 |
| 7-101 | (dir) | | | 0.72 | 0.61 | 26.9 | 41.9 |
| 210 | (lat) | | | 0.60 | 1.23 | 26.9 | 9.0 |
| 210 | (lon) | 16.5 | 3.2 | 0.57 | 1.23 | 26.9 | 5.4 |
| 210 | (dir) | | | 0.60 | 0.62 | 26.9 | 19.7 |
| 7-68 | (lat) | | | 0.67 | 1.36 | 26.9 | 35.9 |
| 7-68 | (lon) | 18.2 | 3.6 | 0.72 | 1.36 | 26.9 | 91.7 |
| 7-68 | (dir) | | | 0.66 | 0.68 | 26.9 | 30.2 |
| 5 | (lat) | | | 0.78 | 1.65 | 26.9 | 19.6 |
| 5 | (lon) | 22.2 | 4.5 | 0.68 | 1.65 | 26.9 | 44.1 |
| 5 | (dir) | | | 0.78 | 0.83 | 26.9 | 12.4 |
| 10 | (lat) | | | 0.76 | 2.10 | 26.9 | 15.4 |
| 10 | (lon) | 28.2 | 7.1 | 1.03 | 2.10 | 26.9 | 99.4 |
| 10 | (dir) | | | 0.87 | 1.05 | 26.9 | 59.3 |

of inertia on the response to turbulence are the same as the effects of the inertia differences on the response to control inputs.

Based on these findings, a single model was adopted for the lateral and longitudinal gust inputs. The required scale factors of Eqs. (10) and (11) were obtained by fitting the empirical results for $K$ in Table 4. The scale factors are for lateral and longitudinal

$$K_{\delta_g} = 0.04096\sigma_{w_g}^{0.3735} \tag{12}$$

for directional

$$K_{\delta_g} = 0.05986\sigma_{w_g}^{0.3507} \tag{13}$$

for collective

$$K_{\delta_g} = 0.01286\sigma_{w_g}^{0.2931} \tag{14}$$

The final gust transfer function models (output in inches of mixer) obtained from Eqs. (12), (13), and (14) are for lateral/longitudinal

$$G_{\delta_g} = 0.08192\sigma_{w_g}^{-0.6265}\left(\frac{\sqrt{\dfrac{\sigma^2 U_o}{\pi L}}}{s + \dfrac{2U_o}{L}}\right) \tag{15}$$

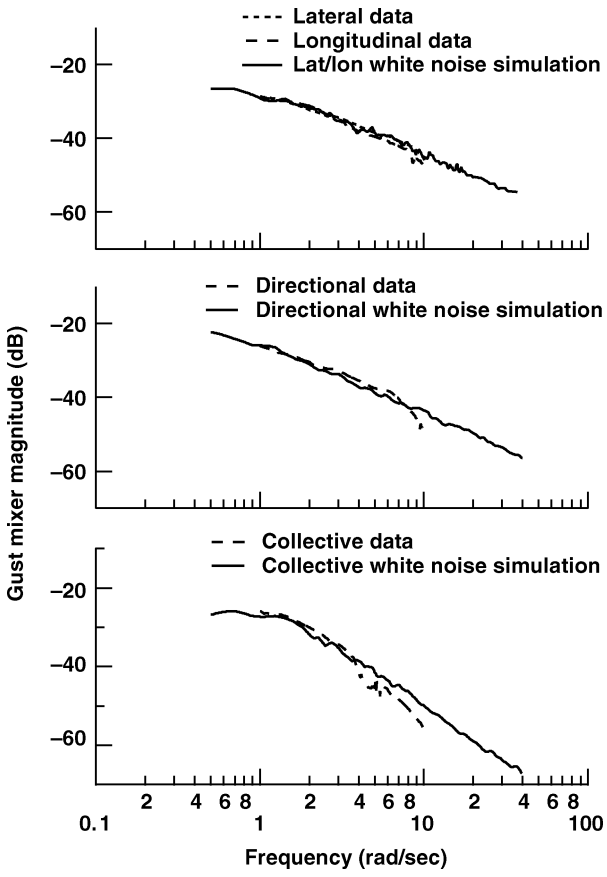


**Fig. 13. Verification of gust model for light turbulence.**

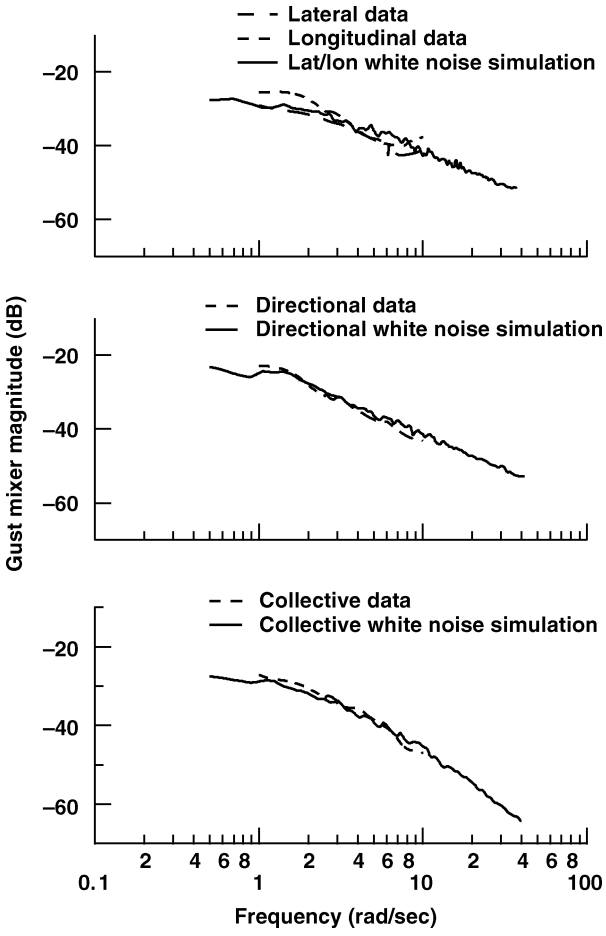


**Fig. 14. Verification of gust model for strong turbulence.**

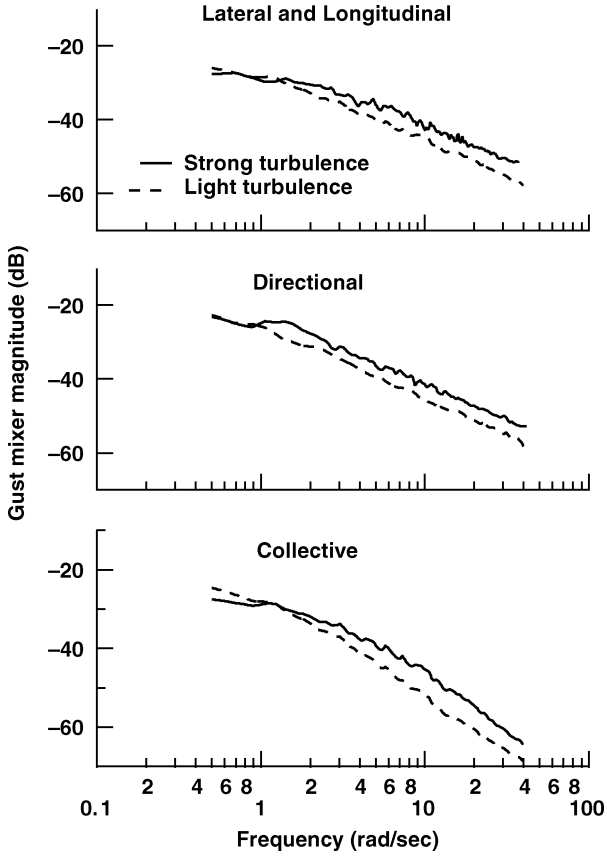


**Fig. 15. Gust excitation model for varying levels of turbulence.**

for directional

$$G_{\delta_g} = 0.08464\sigma_{w_g}^{-0.6493}\left(\frac{\sqrt{\frac{\sigma^2 U_o}{\pi L}}}{s+\frac{U_o}{L}}\right) \tag{16}$$

for collective

$$G_{\delta_g} = 0.01286\sigma_{w_g}^{-0.7069}\left(\frac{\sqrt{\frac{3\sigma^2 U_o}{\pi L}}\left(s+33.91\frac{U_o}{L}\right)}{\left(s+1.46\frac{U_o}{L}\right)\left(s+9.45\frac{U_o}{L}\right)}\right) \tag{17}$$

A check of the gust models was conducted by executing a white noise simulation. Figures 13 and 14 compare the resulting simulated gust mixer inputs against the gust mixer inputs derived from the flight-test data. These models show a good fit over the desired frequency range of 1.0–10 rad/sec. Autospectrum plots of the outputs of the gust models for two of the levels of turbulence investigated are presented in Fig. 15, and show that the autospectrum output of each model increases with increasing turbulence as expected.

## Discussion and Remarks

To utilize the gust model in a simulation, white noise sources are used as input signals into the gust transfer functions, which produce output signals (mixer input in inches) that have autospectra that are nearly equivalent to the measured results (e.g., Figs. 13 and 14). The noise sources utilized herein were Simulink® white noise generators with a noise power of 1 and randomly selected seeds for each noise source. To use a random number generator with a mean of zero and a variance of 1, the output must be scaled by the square root of the sampling frequency selected for the simulation (i.e., for a sampling frequency of 100 Hz, the random number signal would be multiplied by 10). The gust models presented here are applicable to a class of helicopters with the same general physical characteristics (i.e., rotor diameter, configuration and gross weight) hovering in the lowest level of the atmospheric boundary layer. Extension to forward flight and higher altitudes needs to be investigated.

It is important to keep in mind that this first attempt at characterizing the aircraft response to turbulence makes no attempt to model the exact details of the rotor response that would be contained in a rotating frame turbulence model. This is an effort to model aircraft control inputs, which generate the aircraft response to turbulence, and not the components of the gust velocities and gradients themselves.

## Conclusions

A system identification approach has been used to extract control system requirements for precision hover in a turbulent environment and develop realistic helicopter gust response models from UH-60 flight test data. Based on the research presented, specific conclusions are:

1) Control system requirements extracted from flight test data are independent of aircraft orientation and show that current ADS-33E-PRF disturbance rejection requirements are too lenient.

2) Inverse methods were successfully employed to extract accurate disturbance models for hover, which exhibit a Dryden form. The circular rotor disc leads to a common model for the pitch and roll axes. Separate models are obtained for the yaw and heave axes.

3) The gust models developed herein for use in piloted inflight or ground-based simulation are scalable with wind speed and turbulence and generate control inputs to the swashplate which produce an equivalent aircraft response to turbulence.

## Acknowledgments

This research was supported by NASA Grant NCC2-5313, NASA Ames Research Center, Moffett Field, CA. The grant technical manager was Dr. Mark B. Tischler of the Flight Control and Cockpit Integration Branch. The research team also acknowledges the assistance of the many members of the Flight Control and Cockpit Integration Branch of the Army/NASA Rotorcraft Division in this effort. MAJ Dave Arterburn of the Aeroflightdynamics Directorate Flight Projects Office was instrumental in completing the flight test associated with this project. The support of Kurt Long, of Naval Air Warfare Center, Aircraft Division, Patuxent River, was deeply appreciated. The authors would also like to thank Professor Ronald A. Hess, University of California, Davis, for his insight and consultation in developing the modeling process used herein.

## References

[1]Anon., "Handling Qualities Requirements for Military Rotorcraft," Aeronautical Design Standard-33 (ADS-33E-PRF), US Army Aviation and Missile Command, March 2000.

[2]Baillie, S. W., and Morgan, J. M., "An In-flight Investigation into the Relationships Among Control Sensitivity, Control Bandwidth and Disturbance Rejection Bandwidth Using a Variable Stability Helicopter," 15th European Rotorcraft Forum, Amsterdam, The Netherlands, September 1989.

[3]McLean, D., *Automatic Flight Control Systems*, Prentice Hall International (UK) Ltd, Hertfordshire, 1990, pp. 127–135.

[4]Reeves, P. M., "A Non-Gaussian Turbulence Simulation," Technical Report AFFDL-TR-69-67, November 1969.

[5]Dahl, H. J., and Faulkner, A. J., "Helicopter Simulation in Atmospheric Turbulence," 4th European Rotorcraft Forum, Stresa, Italy, September 1978.

[6]Hess, R. A., "Rotorcraft Handling Qualities in Turbulence," *Journal of Guidance, Control, and Dynamics*, Vol. 18, (1), January–February 1995.

[7]George, V. V., Gaonkar, G. H., Prasad, J. V. R., and Schrage, D. P., "Adequacy of Modeling Turbulence and Related Effects of Helicopter Response," *AIAA Journal*, Vol. 30, (6), 1992.

[8]Labows, S., "UH-60 Black Hawk Disturbance Rejection Study for Hover/Low Speed Handling Qualities Criteria and Turbulence Modeling," M.S. Thesis, Naval Postgraduate School, Monterey, CA, March 2000.

[9]Technical Manual, TM 55-1520-237-10, with change 3, Operator's Manual for Army UH-60A Helicopter, Headquarters, Department of the Army, October 1998.

[10]Castro, I., and Robins, A., "The Flow Around a Surface-Mounted Cube in Uniform and Turbulent Streams," Central Electricity Generating Board, Marchwood Engineering Laboratories, Marchwood, Southampton, England, January 1976.

[11]Tischler, M. B., and Cauffman, M. G., "Frequency-Response Method for Rotorcraft System Identification: Flight Applications to BO-105 Coupled Rotor/Fuselage Dynamics," *Journal of the American Helicopter Society*, Vol. 37, (3), July 1992, pp. 3–17.

[12]Atencio, A. Jr., "Fidelity Assessment of a UH-60A Simulation on the NASA Ames Vertical Motion Simulator," NASA TM 104016, September 1993.

[13]Moralez, E., Hindson, W. S., Frost, C. R., Tucker, G. E., Arterburn, D. R., Kalinowski, K. F., and Dones, F., "Flight Research Qualification of the Army/NASA RASCAL Variable-Stability Helicopter," Proceedings of the American Helicopter Society 58th Annual Forum, Montréal, Canada, June 2002, pp. 499–514.

[14]Fletcher, J. W., and Tischler, M. B., "Improving Helicopter Flight Mechanics Models with Laser Measurements of Blade Flapping," Proceedings of the American Helicopter Society 53th Annual Forum, Virginia Beach, VA, May 1997, pp. 1467–1494.

[15]Hess, R. A., and Siwakosit, W., "Assessment of Flight Simulator Fidelity in Multiaxis Tasks Including Visual Cue Quality," *Journal of Aircraft*, Vol. 38, (4), July–August 2001.

[16]Woo, H., Peterka, J., and Cermak, J., "Wind Tunnel Measurements in the Wakes of Structures," NASA CR-2806, March 1977.

[17]Anon., "Military Standard Flying Qualities of Piloted Aircraft," MIL-STD-1797A, January 1990.

[18]Costello, M., Gaonkar, G. H., Prasad, J. V. R., and Schrage, D. P., "Some Issues on Modeling Atmospheric Turbulence Experienced by Helicopter Rotor Blades," *Journal of the American Helicopter Society*, Vol. 37, (2), April 1992, pp. 71–75.